

Effects of Dissolved Carbonate on Arsenate Adsorption and Surface Speciation at the Hematite–Water Interface

YUJI ARAI,^{*,†,‡} D. L. SPARKS,[‡] AND J. A. DAVIS[†]

U.S. Geological Survey, MS 465, 345 Middlefield Road, Menlo Park, California 94025, and Department of Plant and Soil Sciences, University of Delaware, Newark, Delaware 19717

Effects of dissolved carbonate on arsenate [As(V)] reactivity and surface speciation at the hematite–water interface were studied as a function of pH and two different partial pressures of carbon dioxide gas [$P_{\text{CO}_2} = 10^{-3.5}$ atm and ~ 0 ; CO_2 -free argon (Ar)] using adsorption kinetics, pseudo-equilibrium adsorption/titration experiments, extended X-ray absorption fine structure spectroscopic (EXAFS) analyses, and surface complexation modeling. Different adsorbed carbonate concentrations, due to the two different atmospheric systems, resulted in an enhanced and/or suppressed extent of As(V) adsorption. As(V) adsorption kinetics [4 g L^{-1} , $[\text{As(V)}]_0 = 1.5 \text{ mM}$ and $I = 0.01 \text{ M NaCl}$] showed carbonate-enhanced As(V) uptake in the air-equilibrated systems at pH 4 and 6 and at pH 8 after 3 h of reaction. Suppressed As(V) adsorption was observed in the air-equilibrated system in the early stages of the reaction at pH 8. In the pseudo-equilibrium adsorption experiments [1 g L^{-1} , $[\text{As(V)}]_0 = 0.5 \text{ mM}$ and $I = 0.01 \text{ M NaCl}$], in which each pH value was held constant by a pH-stat apparatus, effects of dissolved carbonate on As(V) uptake were almost negligible at equilibrium, but titrant (0.1 M HCl) consumption was greater in the air-equilibrated systems ($P_{\text{CO}_2} = 10^{-3.5}$ atm) than in the CO_2 -free argon system at pH 4–7.75. The EXAFS analyses indicated that As(V) tetrahedral molecules were coordinated on iron octahedral via bidentate mononuclear ($\approx 2.8 \text{ \AA}$) and bidentate binuclear ($\approx 3.3 \text{ \AA}$) bonding at pH 4.5–8 and loading levels of $0.46\text{--}3.10 \mu\text{M m}^{-2}$. Using the results of the pseudo-equilibrium adsorption data and the XAS analyses, the pH-dependent As(V) adsorption under the $P_{\text{CO}_2} = 10^{-3.5}$ atm and the CO_2 -free argon system was modeled using surface complexation modeling, and the results are consistent with the formation of nonprotonated bidentate surface species at the hematite surfaces. The results also suggest that the acid titrant consumption was strongly affected by changes to electrical double-layer potentials caused by the adsorption of carbonate in the air-equilibrated system. Overall results suggest that the effects of dissolved carbonate on As(V) adsorption were influenced by the

reaction conditions [e.g., available surface sites, initial As(V) concentrations, and reaction times]. Quantifying the effects of adsorbed carbonate may be important in predicting As(V) transport processes in groundwater, where iron oxide-coated aquifer materials are exposed to seasonally fluctuating partial pressures of $\text{CO}_2(\text{g})$.

Introduction

Arsenic (As) is a toxic metalloid in oxic-reduced terrestrial/aquatic environments derived from indigenous sources (e.g., weathering of As minerals and geothermal discharge) and industrial/agricultural inputs (e.g., use of arsenical pesticides and coal fly ash) (1). Recent changes in regulations lowering the maximum concentration level of total As in drinking water to $10 \mu\text{g L}^{-1}$ increase the need for environmental protection measures and for research by the scientific community. To better predict the environmental fate of As in soil/water environments, it is vital to understand rate-limiting processes such as adsorption processes in soils and sediments. Because the bioavailability/solubility of As could depend on solid state speciation upon changes in redox status, ionic strength, pH, and microbial communities, a detailed understanding of As surface speciation is extremely important for assessing environmental risks and developing remediation strategies.

Many researchers have investigated arsenite [As(III)] and As(V) adsorption reactions and surface speciation on major soil minerals (i.e., metal oxyhydroxides and phyllosilicate minerals) using various macroscopic and spectroscopic techniques. Arsenate is strongly adsorbed at acidic pH values on amorphous $\text{Al}(\text{OH})_3$, $\alpha\text{-Al}_2\text{O}_3$, ferrihydrite, and hematite (2–5). Several spectroscopic studies [e.g., extended X-ray adsorption fine structure spectroscopy (EXAFS) and diffuse reflectance and attenuated total reflectance Fourier-transform infrared spectroscopies (DRIFT and ATR-FTIR, respectively)] and macroscopic studies [e.g., electrophoretic mobility (EM) and titration measurements] have revealed inner-sphere bidentate binuclear and/or monodentate As(V) complexes on ferrihydrite, goethite, amorphous iron and aluminum oxides, and the bayerite polymorph (3, 6–10), and both inner-sphere and outer-sphere As(III) complexes on aluminum oxides (3, 11).

While these studies have provided insight into the coordination environments of adsorbed As(III and V) at the soil mineral–water interfaces, the adsorption mechanisms are often postulated/ modeled without considering (1) protonation environments of As surface species and (2) adsorbed/dissolved carbonate species at the mineral–water interfaces.

The nature of protonation of the surface species highly influences the strength of the sorption complexes and their chemical reactivity at the mineral surfaces (12).

Several FTIR studies have indicated that adsorbed tetrahedral anions (i.e., phosphate) might have protonated and nonprotonated species when they are sorbed on iron oxyhydroxide surfaces (13–15). These spectroscopic results suggest that a similar tetrahedral anion such as AsO_4 (e.g., hydrolysis constants) could be associated with protons on metal oxide surfaces.

A typical range of total carbonate in the groundwater in United States is reported as $0.5\text{--}8 \text{ mM}$ (16), suggesting that carbonate ions might have a significant role in the contaminant retention/release via competitive adsorption. Adsorbed carbonate ions alter the surface charge properties of metal oxides (17, 18) via inner-sphere monodentate mononuclear surface species (19), and some experimental studies

* Corresponding author: address: U.S. Geological Survey, Water Resource Division, 345 Middlefield Rd., MS 465, Menlo Park, CA 94025; phone: (650) 329-4520; fax: (650) 329-4327; e-mail: yarai@usgs.gov.

[†] U.S. Geological Survey.

[‡] University of Delaware.

indicate that carbonate enhanced or suppressed oxyanion (i.e., chromate, selenate, and sulfate) uptake occurs on metal oxide surfaces (20, 21). On the basis of these experimental results, it is plausible that carbonate could influence the arsenate uptake on soil mineral surfaces. Comprehensive knowledge of the molecular scale chemical speciation (i.e., protonation and coordination environment of surface complexes) as a function of dissolved/adsorbed carbonate will greatly aid in predicting the reactivity of arsenate in carbonate-rich groundwater and the vadose zone.

Arsenate is known to strongly interact with iron oxides in soils, sediments, aquifer materials, and mine waste (22–26). Hematite ($\alpha\text{-Fe}_2\text{O}_3$), which is commonly present in subtropical to tropical soils, was chosen as a model soil adsorbent in this study. The effects of carbonate on As(V) adsorption kinetics and pseudo-equilibrium adsorption experiments, titration experiments, and EXAFS measurements were coupled to elucidate the As(V) adsorption mechanisms at the hematite–water interface. The results of spectroscopic analyses and the titration data were used for surface complexation modeling to accurately understand the stoichiometric reaction and protonation environment of the surface species.

Experimental Procedures

Materials. High surface area hematite ($\alpha\text{-Fe}_2\text{O}_3$) was synthesized according to the method of Schwertmann and Cornell (27). Five hundred milliliters of 0.2 M ferric nitrate solution was prepared at pH 8 and heated at 98 °C for 7 days. The precipitate was washed several times with deionized water by centrifugation and decantation until the nitrate concentration was reduced to <0.003 mM. The hematite paste was freeze-dried. The five-point N_2 –Brunauer–Emmett–Teller (BET) surface area was $56 \text{ m}^2 \text{ g}^{-1}$. Sodium arsenate ($\text{Na}_2\text{HAsO}_4 \cdot 7\text{H}_2\text{O}$, Baker) stock solutions (10 mM) were prepared in 0.01 M NaCl using MilliQ water (18 Ω), and the same stock solutions were also prepared using boiled MilliQ water for adsorption experiments in the absence of CO_2 .

Pseudo-equilibrium Arsenate Adsorption Experiments.

Arsenate adsorption experiments with hematite [1 g L^{-1} [As(V)] $_0 \approx 0.5$ mM and $I = 0.01$ M NaCl] were conducted as a function of pH (4–7.75) under ambient air [with the partial pressure of carbon dioxide gas (P_{CO_2}) = $10^{-3.5}$ atm] or CO_2 -free argon (Ar) atmospheres. For the experiments in the open air system, specific amounts of 10 mM sodium bicarbonate solution were added to freshly prepared hematite stock suspensions (1.25 g L^{-1} in 0.01 M NaCl) and As(V) solutions to facilitate atmospheric CO_2 equilibration of the solutions at the desired pH values. pH values of these experimental solutions were stabilized under the humidified air for 24 h using a stirred pH stat apparatus prior to the As(V) adsorption experiments. For the CO_2 -free experiments, boiled MilliQ water was used to prepare all reagents in 0.01 M NaCl. To minimize adsorbed carbonate ions on hematite surfaces, the pH of hematite suspensions was initially adjusted to ≈ 4 and purged with humidified Ar gas for 24 h. pH values were readjusted using a CO_2 -free 0.1 M NaOH solution and then equilibrated for 24 h. Similar pH adjustment and CO_2 removal processes for the sodium arsenate stock solutions were performed prior to the adsorption experiments. An appropriate amount of As(V) stock solution was then added to ensure an initial As concentration of ≈ 0.5 mmol. The samples were reacted for 24 h on a stirred pH stat apparatus, and the volume of titrant (i.e., 0.1 M HCl) consumption to hold the pH constant was recorded. Ten milliliters of the suspension was passed through 0.22 μm Millex-GX filters (Millipore Corp., Bedford, MA), and filtrates were analyzed for total As using inductively coupled plasma–atomic emission spectroscopy (ICP-AES).

Arsenate Adsorption Kinetics. Arsenate adsorption kinetic measurements with hematite were conducted at pH 4,

6, and 8 under the $P_{\text{CO}_2} = 10^{-3.5}$ atm or the Ar atmosphere in the presence of excess surface sites [i.e., 4 g L^{-1} hematite [As(V)] $_0 \sim 1.5$ mM and $I = 0.01$ M NaCl], pH adjustments and Ar/air equilibration of the stock solutions were as described above. Arsenate adsorption kinetic experiments were carried out by slowly adding sodium arsenate stock solutions (i.e., 10 mL addition every 10 s) into the hematite suspensions to ensure an initial As(V) concentration of ≈ 1.5 mmol. The mineral suspensions were stirred at 300 rpm at 298 K. Ten milliliters of mineral suspension was periodically collected (i.e., 5, 10, 15, and 30 min and 1, 2, 3, 6, 12, and 24 h) and then passed through the 0.22 μm filters. The filtrates were analyzed for total As and Fe using ICP-AES.

Extended X-ray Absorption Fine Structure Spectroscopic

Analyses. All XAS samples were prepared under $P_{\text{CO}_2} = 10^{-3.5}$ atm using the same experimental methods described under Arsenate Adsorption Kinetics. To study the effects of loading levels and pH on the As(V) surface speciation, the following reaction conditions were used: [As] $_0 = 0.3, 0.5, 0.7,$ and 1.5 mM; pH 4.5, 6, and 8; and suspension density = 4 and 8 g L^{-1} . Thirty milliliters of the As(V)-reacted hematite suspensions was collected and centrifuged at $11950g$ for 10 min at 20 °C. The paste was recovered and loaded in Teflon sample holders, which were then sealed with Kapton tape (CHR Industries) and kept at 5 °C prior to the XAS data collection. Arsenic K-edge (11867 eV) XAS spectra were collected on beamline X-11A at the National Synchrotron Light Source (NSLS), Brookhaven National Laboratory, Upton, NY. The electron storage ring was operated at 2.528 GeV with a current range of 130–250 mA. The XAS spectra were collected in fluorescence mode with a Lytle detector filled with krypton gas. The EXAFS spectra were collected in 0.5–10 eV steps between the pre-edge to extended regions. The ionization chamber (I_0) was filled with 90% N_2 and 10% Ar. As an internal standard, the arsenic K-edge of sodium arsenate salt was run simultaneously with adsorption samples to check for potential energy shifts during the run. A Ge filter was used to remove elastically scattered radiation from the fluorescence emissions. The monochromator consisted of two parallel Si(111) crystals with a vertical entrance slit of 0.5 mm. The Teflon sample holder was oriented at 45° to the unfocused incident beam. We performed data collection of the sorption samples at room temperature.

XAS data reduction and analyses were performed with WinXas 2.0 (28) using the following procedures. First, several spectra were averaged. The averaged spectra were normalized with respect to E_0 determined from the second derivative of the raw spectra, and then the total atomic cross-sectional absorption was set to unity. A low-order polynomial function was fit to the pre-edge region and the postedge region. Next, the data were converted from E -space to k -space and weighted by k^3 to compensate for dampening of the XAFS amplitude with increasing k space. Fourier transformation was then performed over the Δk space range of 11–12 Å^{-1} to obtain the radial structural functions (RSF). Final fitting of the spectra was done on Fourier-transformed k^3 -weighted spectra in R space. The FEFF702 code reference (29) was utilized to calculate single-scattering theoretical spectra and phase shifts for As–O and As–Fe backscatters using an input file based on the structural refinement of scorodite ($\text{FeAsO}_4 \cdot \text{H}_2\text{O}$) (30) with two Fe atoms. During fitting, the values of coordination number (CN) and interatomic distance (R) of the As–O and As–Fe shells were allowed to vary, as well as a single E_0 for all sets of backscattering atoms. Two different As–Fe single-scattering paths were independently fit. The Debye–Waller factors (σ^2) of the As–O shells were also allowed to vary, but those of the As–Fe shells were fixed at 0.007 Å^2 . When allowed to vary, the σ^2 of the As–Fe shells showed no trends for different samples (e.g., as a function of pH and loading levels), and we therefore used the average

TABLE 1. Reaction Conditions of XAS Samples and Structural Parameters from the Least-Squares Analyses of As K-Edge EXAFS Spectra

reaction conditions (pH, suspension density, [As(V)] ₀ , Γ) ^b	As–O ^a			As–Fe1 ^a			As–Fe2 ^a			ΔE ^c (eV)
	CN ^c	R ^d (Å)	σ ² ^e (Å ²)	CN	R (Å)	σ ² ^f (Å ²)	CN	R (Å)	σ ² ^f (Å ²)	
pH 8.0, 4 g L ⁻¹ , 0.5 mM, 0.83 μM m ⁻²	4.37	1.68	0.0012	0.82	2.81	0.007	0.71	3.27	0.007	3.68
pH 8.0, 8 g L ⁻¹ , 0.3 mM, 0.45 μM m ⁻²	4.64	1.69	0.0013	0.62	2.79	0.007	1.17	3.27	0.007	4.44
pH 6.1, 8 g L ⁻¹ , 1.5 mM, 1.83 μM m ⁻²	4.57	1.69	0.0013	0.54	2.86	0.007	1.31	3.29	0.007	3.76
pH 6.1, 8 g L ⁻¹ , 0.5 mM, 1.75 μM m ⁻²	4.27	1.68	0.0012	0.52	2.82	0.007	1.48	3.26	0.007	2.90
pH 4.5, 4 g L ⁻¹ , 1.5 mM, 3.10 μM m ⁻²	4.51	1.69	0.0013	0.72	2.78	0.007	1.93	3.23	0.007	3.42
pH 4.5, 8 g L ⁻¹ , 0.7 mM, 2.62 μM m ⁻²	4.61	1.68	0.0012	0.70	2.78	0.007	1.53	3.26	0.007	3.70
pH 4.5, 8 g L ⁻¹ , 0.5 mM, 2.23 μM m ⁻²	4.22	1.68	0.0012	0.47	2.84	0.007	1.43	3.26	0.007	3.77

^a Fit quality confidence limit for parameters: As–O and As–Fe shells, R, $\pm 0.30\%$; As–O shell, CN, $\pm 12\%$; As–Fe shells, CN, $\pm 38\%$. ^b [As(V)]₀ = initial As(V) concentrations; Γ = loading level. ^c CN = coordination number. ^d R = interatomic distance. ^e σ² = Debye–Waller factor. ^f Fixed parameter.

values (0.007 Å²) in the final fitting procedure to reduce the number of free parameters. A fixed value of 0.9 was used for the amplitude reduction factor (S₀²). Errors of CN and R for the As–O/Fe shells were estimated by comparison of the EXAFS fit results to the values given by Kitahama et al. (30). The accuracies were $\pm 0.30\%$ for R_{As–O/As–Fe}, $\pm 12\%$ for CN_{As–O}, and $\pm 38\%$ for CN_{As–Fe}.

Surface Complexation Modeling. FITEQL 4.0 (31) was used to determine the best fit of various As(V) surface complexation reactions or combinations of reactions to the experimental As(V) adsorption data. The Davies equation was used for activity correction of aqueous species only. Relative errors of 1% in the concentrations of surface sites, total As(V), and adsorbed As(V) and relative errors of 5% in log [H⁺] and log [H₂CO₃] were used as FITEQL input values. Aqueous speciation thermodynamic data for As(V) used in the modeling were from Nordstrom and Archer (32).

Results and Discussion

Extended X-ray Absorption Fine Structure Spectroscopic Analyses. Figure 1a shows the k³-weighted EXAFS spectra of As(V)-adsorbed hematite samples. The spectra show strong sinusoidal oscillations resulting from O-shell backscattering. The oscillations at 4–8 Å⁻¹ are slightly different from those of a sodium arsenate(aq) spectrum (3), but similar to those of other As(V)-adsorbed iron oxyhydroxides (8), suggesting the As(V) inner-sphere complexation mechanisms on iron octahedral structures. Fourier-transformed k³-weighted spectra (uncorrected for phase shift) show the quantitative estimation of interatomic distances between As and next neighboring atoms in the As(V) adsorption samples (Figure 1b). The structural parameters obtained from the linear least-squares fits of the EXAFS data are shown in Table 1. Interatomic distances of the As–O shell (~1.69 Å) after correction for phase shifts and estimated coordination numbers (Table 1) indicate that AsO₄ tetrahedral molecular structures are present in all samples. In addition to the major As–O shell, there are two As–Fe shells as indicated by the vertical lines As–Fe1 and As–Fe2 (Figure 1b). Although the intensity of the major As–Fe1 shell varied somewhat for different reaction conditions, the As–Fe2 shells were consistently present for the reaction conditions we studied (i.e., pH 4–8 and Γ = 0.67–3.1 μM m⁻²), suggesting the presence of mixed As(V) bonding environments on the hematite surfaces. The radial distance of one of the As–Fe2 shells was ~3.29 Å, and this is in good agreement with the bidentate binuclear As–Fe distances previously reported on As(V) reacted iron oxyhydroxide (8). It seems possible to assign the interatomic distance of ~3.3 Å for tilted (As–O–Fe angle of ~125°) monodentate mononuclear surface species. To consider the tilted molecular configuration, it is reasonable

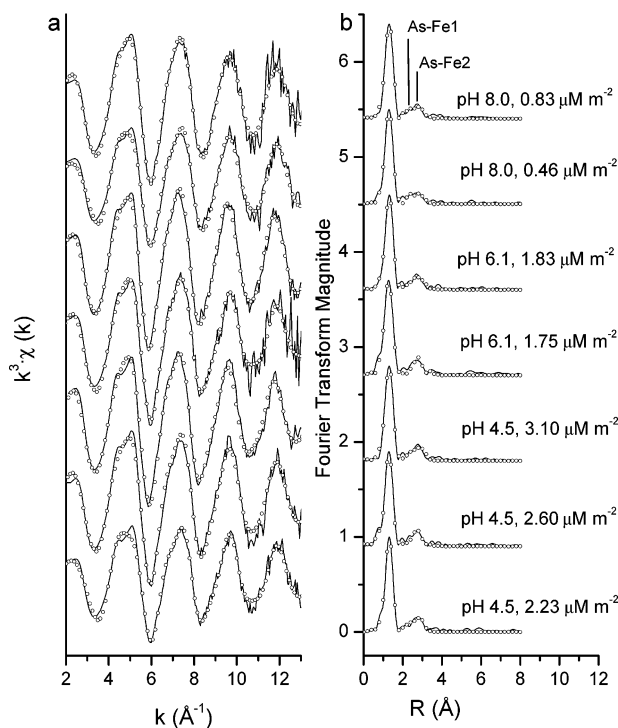


FIGURE 1. (a) Normalized, background-subtracted k³-weighted As K-edge EXAFS spectra of As(V) adsorbed hematite samples. Solid lines are the experimental data, and the open circles represent the theoretical fit to the data. (b) Fourier-transformed k³-weighted As K-edge EXAFS spectra of As(V) adsorbed hematite (solid lines) and nonlinear least-squares fits (open circles).

to assume that the arsenate tetrahedral molecules are hydrogen bonded to the Fe octahedral surfaces (i.e., proton association). However, the recent in-situ FTIR study suggested that the adsorbed phosphate molecules are not associated with proton(s) at the surface of iron oxide at pH 7.5 and are forming nonprotonated bidentate binuclear surface species (13). Considering the PO₄ as an analogue of AsO₄, we exclude the possibility of tilted As(V) monodentate mononuclear surface species. The minor As–Fe1 distance occurred at 2.78–2.86 Å, which is close to the values reported by several researchers (6, 7) for the As(V) bidentate mononuclear configurations on the iron octahedral.

Overall, our EXAFS analyses showed the presence of at least two surface species (i.e., bidentate mononuclear and bidentate binuclear complexes) coexisting under the reaction conditions we studied.

Arsenate Adsorption Kinetics. Figure 2 shows the pH and [carbonate] effects on As(V) adsorption kinetics at the hematite surface, and the magnified data plots in each figure

represent the initial 3 h of reactions. Adsorption reactions in air and Ar show an initial fast adsorption process that is followed by a slower uptake process with increasing time at pH 4, 6, and 8. Similar biphasic As(V) adsorption kinetic data have been reported on other metal oxide surfaces (2, 4, 33–35). Because bicarbonate is known to promote iron dissolution from hematite surfaces (36), we also monitored total dissolved Fe during the adsorption experiments. Fe(III)–As(V) ion activity product calculations based on the dissolved total Fe concentration [at most of 0.04 mg L⁻¹ (±0.97)] and As concentrations suggested that the systems were below saturation with respect to ferric arsenate precipitates. This implies that the observed uptake of As(V) can be discussed by adsorption reactions.

Total As(V) uptake after 24 h was consistently lower in the closed argon (i.e., CO₂-free) system at three different pH values (Figure 2), indirectly suggesting that carbonate might have enhanced the As(V) adsorption. Carbonate-enhanced SeO₄ and SO₄ uptake on goethite surfaces via proton coadsorption reactions has been reported earlier by Wijnja and Schulthess (20). The carbonate adsorption on metal oxide surfaces is known to decrease surface charge density over a wide pH range due to specific adsorption of carbonate (18, 19), resulting in lower zeta potentials for minerals. Carbonate adsorption on iron oxides is pH dependent and is typically maximized at pH ~6 (37, 38). Su and Suarez (19), Wijnja and Schulthess (40), and Villalobos and Leckie (39) previously suggested monodentate carbonate species on goethite surfaces, and it is possible that similar monodentate mononuclear carbonate surface species are forming on hematite surfaces. At first glance, there is no straightforward explanation for enhanced As(V) adsorption on carbonate-adsorbed hematite surfaces with lower charge. In our experimental systems before the introduction of AsO₄ solutions, mineral–water interfacial environments were (1) (bi)carbonate adsorbed and hydroxyl/water-linked Fe polyhedron in the open-air system and (2) only hydroxyl/water-linked Fe polyhedral in the closed argon (i.e., CO₂ free) systems. Interestingly, the ionic bond strengths in these two different terminal ≡Fe–O bonds [i.e., ≡Fe–OCO₂(H)²⁻ and ≡Fe–OH(H)] are largely different, suggesting that different reactive sites may be available for dissolved AsO₄. McBride earlier discussed that shared charged values (i.e., values determined by dividing the valence state of the central atom by the number of bonded O atoms) of different oxyanions affect the strength of the metal–oxyanion ionic bond (41). For smaller “shared charge”, the effective negative charge residing on each O atom is greater and stronger metal–oxyanion ionic bonds form (41). The shared charge value is 1.0 for OH⁻ and 1.33 for CO₃²⁻, suggesting the ionic bond strength of the terminal ≡Fe–O bond is weaker for the monodentate mononuclear linked carbonate than that of the surface hydroxyl group. Because the shared charged value of AsO₄³⁻ (i.e., 1.25) is lower than that of CO₃²⁻, but higher than that of OH⁻, dissolved AsO₄ anions may displace adsorbed (bi)carbonate ions more effectively than the surface hydroxyl groups attached to Fe polyhedron. This could result in the enhanced As(V) adsorption on the carbonate-adsorbed hematite surfaces in the open-air system. This ionic bond hypothesis was postulated on the basis of the results of the previous FTIR studies (18, 19, 39, 40) that suggested the presence of monodentate mononuclear carbonate surface species on Fe polyhedron.

This hypothesis for carbonate-enhanced As(V) adsorption is consistent with the kinetic adsorption data at pH 4 and 6. However, the initial <2 h of As(V) adsorption at pH 8 shows a much slower As(V) uptake in the air than in the argon system (a magnified data plot in Figure 2c). This can be attributed to the competitive adsorption between dissolved carbonate and As(V) in the open system. Unlike the pH 4

open system, the pH 8 open system contains >1 mM dissolved carbonate, and at this concentration, carbonate may compete for the As(V) adsorption sites. A recent surface complexation modeling study predicted carbonate competition with As(V) adsorption on ferrihydrite surfaces (42). In addition, Wilkie and Hering also found a slight decrease in As(V) adsorption on ferrihydrite at pH 9 (43).

pH Dependence of Arsenate Adsorption and Surface Complexation Modeling. Figure 3 shows As(V) adsorption on hematite as a function of pH. Due to experimental design considerations, the reaction conditions (1 g L⁻¹ and [As]₀ = 0.5 mM) of the pseudo-equilibrium sorption experiments were different from those of the kinetic experiments (4 g L⁻¹ and [As]₀ = 1.5 mM). Arsenate adsorption decreases with increasing pH from 4 to 8, and there were no significant differences in the As(V) uptake observed after 24 h in the open air and argon systems. Overall, the pH dependence of As(V) adsorption was in good agreement with previous As(V) adsorption data on Fe oxide surfaces (4). Fe(III)–As(V) ion activity product calculations based on the dissolved total Fe [at most of 0.64 mg kg⁻¹ (±0.31)] and As concentrations suggested that the systems were undersaturated with respect to ferric arsenate precipitates. It seems that the adsorbed and/or dissolved carbonate had no effects on the pseudo-equilibrium As(V) adsorption data, but an interesting difference occurred in the titrant consumption data. The titrant (0.1 M HCl) consumption was always greater in the air-equilibrated system than in the CO₂-free Ar system (Table 2), suggesting that the release of hard base ligand (e.g., OH⁻ and CO₃²⁻) was facilitated by the presence of carbonate during the As(V) uptake. The increase in negative charge at the surface due to carbonate adsorption is likely responsible for this phenomenon (18, 19).

We have previously attempted to understand the coordination and protonation environments of the AsO₄ surface species using deuterium exchange/ATR-FTIR spectroscopy. However, the interpretation of the asymmetric As–O ν₃ vibrational modes was inconclusive due to interference from the absorption band of hematite. Moreover, the surface complex assignment based on the ν₃ vibration splittings would not be possible because these peaks arise from mixed coordination environments (i.e., bidentate mononuclear and bidentate binuclear complexes) that were suggested in the XAS analyses. Therefore, we used surface complexation modeling in conjunction with the titration data during the pseudo-equilibrium adsorption reactions in this study to understand the protonation environment of the adsorbed As(V) surface species.

The triple-layer model was used to describe As(V) adsorption on hematite as a function of pH and in the presence and absence of dissolved carbonate. The surface site density, acidity constants, electrolyte ion pair formation constants, and other electrical double-layer parameters for hematite were taken from Sahai and Sverjensky (44) and are given in Table 3. Adsorption constants for the carbonate anion (Table 3) were taken from a fit of the carbonate sorption data of Kohler et al. (37). The carbonate surface reaction stoichiometry and modeling approach are similar to that of Villalobos and Leckie for carbonate adsorption on goethite (39).

A one-site model was used to describe the As(V) adsorption data. As indicated above, the XAS data clearly demonstrate that As(V) forms bidentate bonds with iron octahedra. However, for illustrative purposes, both bidentate and monodentate As(V) surface complex formation reactions were tested for “goodness-of-fit” to the adsorption data. FITTEQL output includes a goodness-of-fit parameter, WSOS/DF, which is the weighted sum of squares of the difference in value between model simulations and experimental data

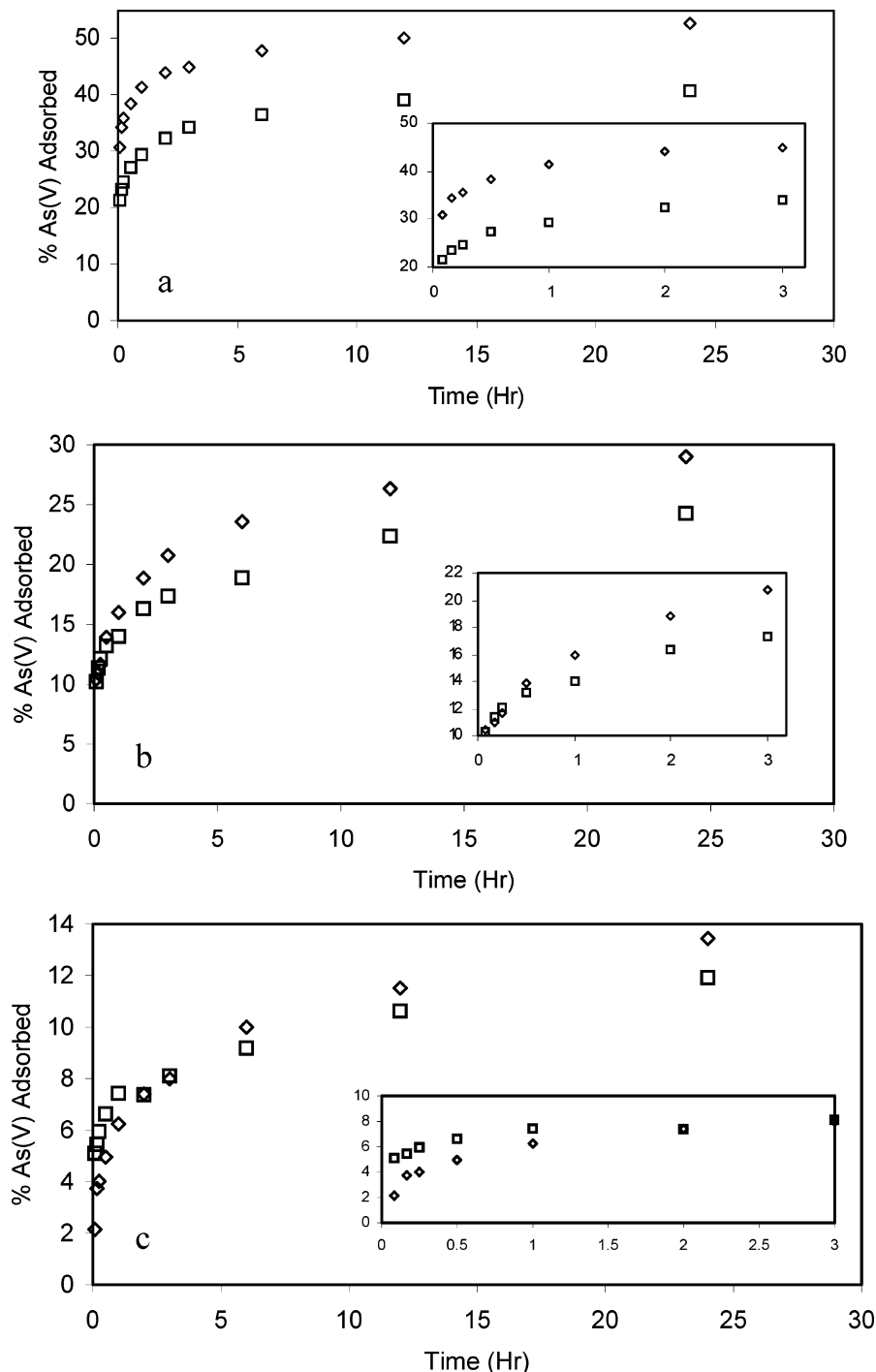


FIGURE 2. Arsenate adsorption kinetics at the hematite–water interfaces under the open air ($P_{\text{CO}_2} = 10^{-3.5}$) and the CO_2 -free argon systems at pH 4 (a), 6 (b), and 8 (c). Open-diamond and -square symbols represent the data collected in air and argon, respectively. The magnified data plots represent the initial 3 h of reactions for each panel. The reaction conditions are $4 \text{ g L}^{-1} [\text{As(V)}]_0 \sim 1.5 \text{ mM}$ and $I = 0.01 \text{ M NaCl}$. Total aqueous carbonate concentrations $[\text{CO}_3^{2-}, \text{H}(\text{CO}_3)^-, \text{H}_2(\text{CO}_3)^0(\text{aq}), \text{Na}(\text{CO}_3)^-, \text{NaH}(\text{CO}_3)^0]$ of the hematite suspensions at equilibrium with respect to $P_{\text{CO}_2} = 10^{-3.5} \text{ atm}$ at pH 4, 6, and 8 are approximately 0.11, 0.1, and 5.56 mM, respectively.

points divided by the degrees of freedom (31). Lower values of WSOS/DF mean the proposed model is a better fit to the experimental data; WSOS/DF will be referred to as “fit” below.

As a first step, the experimental data for As(V) adsorption under an Ar atmosphere were simulated with a single surface complexation reaction, and the fit of each reaction to the experimental was recorded for comparison (Table 4). For surface species with a net charge, a choice is made as to how to correct the mass law for the free energy of adsorption associated with electrostatic attraction or repulsion. The net charge can be approximated as located within the surface

plane of the triple-layer model (σ_0) or within the mean plane of adsorbed ions (σ_β), or the charge can be distributed between the planes, as was demonstrated in the modeling of carbonate anion adsorption (39). For example, consider the arsenate bidentate mononuclear surface species in reaction 1 (Table 4), which has a net charge of -1 . Simulations were compared with the charge of -1 located in the surface plane (reaction 1) or in the β plane (reaction 2) or distributed between these two planes (reactions 3 and 4). Among those four reactions, the best fit (29.5) was obtained with the charge in the β plane (reaction 2, Table 4). Reaction 5 included an

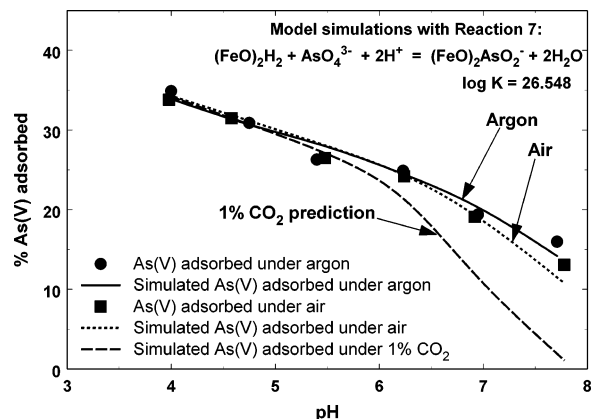


FIGURE 3. Pseudo-equilibrium As(V) adsorption on hematite as a function of pH under the open air ($P_{CO_2} = 10^{-3.5}$) and the CO_2 -free argon systems. The reaction conditions are $1 \text{ g L}^{-1} [As(V)]_0 \approx 0.5 \text{ mM}$ and $I = 0.01 \text{ M NaCl}$. Surface complexation model fit to the experimental data for As(V) adsorption in the CO_2 -free argon system using reaction 7 (Table 4) is shown as a solid curve. Predicted As(V) adsorption in the presence of carbonate (air or 1% P_{CO_2}) is shown as dashed curves.

TABLE 2. Experimental Titrant (0.1 M HCl) Consumption Data during the Pseudo-equilibrium Adsorption Experiments and the Predicted Titrant Consumption Data Based on Surface Complexation Modeling (Reaction 7)

pH	exptl 0.1 M HCl consumption (mol)		simulated 0.1 M HCl consumption (mol)	
	air ($P_{CO_2} = 10^{-3.5} \text{ atm}$)	argon	air ($P_{CO_2} = 10^{-3.5} \text{ atm}$)	argon
4.00	8.3×10^{-6}	4.3×10^{-6}	9.4×10^{-6}	8.2×10^{-6}
4.60	8.9×10^{-6}	6.1×10^{-6}	1.06×10^{-5}	8.9×10^{-6}
5.5	8.0×10^{-6}	6.3×10^{-6}	1.26×10^{-5}	9.5×10^{-6}
6.25	9.5×10^{-6}	8.5×10^{-6}	1.50×10^{-5}	1.16×10^{-5}
7.00	1.32×10^{-5}	1.09×10^{-5}	1.75×10^{-5}	1.50×10^{-5}
7.75	2.37×10^{-5}	1.52×10^{-5}	1.15×10^{-5}	1.39×10^{-5}

TABLE 3. Hematite Triple-Layer Model Parameters

surface species	exponents in mass law defining the surface species ^a					log K_f ($I = 0$)
	a	b	c	d	e	
$\equiv FeO^-$	1	-1	-1			-11.6
$\equiv FeONa$	1	-1	-1	1		-9.8
$\equiv FeOH_2^+$	1	1	1			6.0
$\equiv FeOH_2^+Cl^-$	1	1	1	-1		7.8
$\equiv FeOCO_2^-$	1	-1	1	-0.29	-0.71	-2.91

^a Mass law for formation of the surface species is $[surface\ species] = K_f [\equiv FeOH]^a [H^+]^b [H_2CO_3]^c \exp\{(-F/RT)(d\Psi_0 + e\Psi_d)\}$. Coefficients for Na^+ and Cl^- are not shown. Inner layer capacitance, $C_1 = 0.9 \text{ farad/m}^2$; outer layer capacitance, $C_2 = 0.2 \text{ farad/m}^2$; total surface sites = 22 sites/ nm^2 . Parameters based on values given in Sverjensky and Sahai (44), except for the carbonate binding reaction, given by the fit to the experimental data of Kohler et al. (37).

additional proton in the reaction to form an uncharged bidentate mononuclear surface species; the fit with this reaction was very poor (fit = 4980). Fits to the data with bidentate binuclear surface species followed a similar trend (reactions 6–10), with the best fit (23.9) obtained with a charge of -1 located in the β plane (reaction 7, Table 4).

The fit to the experimental data with various monodentate As(V) surface species was also determined. For the nonprotonated species with a net charge of -2, the best fit (20.3) was obtained with the charge divided between the surface and β planes (reaction 13, Table 4). A reasonable fit (29.5)

was also observed for a singly protonated species with the charge of -1 in the β plane (reaction 16). Even though the monodentate surface species in reactions 13 and 16 fit the adsorption data well, these reactions cannot be justified for a surface complexation model because the EXAFS data clearly show that the primary surface species are bidentate As(V) complexes with Fe octahedral. The surface species in reactions 2 and 7 should be selected for a surface complexation model because they fit the adsorption data well and are consistent with the spectroscopic results. The exponents in the mass laws for reactions 2 and 16 are identical, illustrating that it is impossible to distinguish between certain bidentate mononuclear and monodentate surface species with surface complexation modeling (the same is true for reactions 5 and 17). Covariance of variable also can lead to good fits for proposed surface species. For example, reaction 13 differs from reaction 2 only in the exponent for H^+ and in the charge (z) of the electrostatic correction term, $\exp(-z\Psi_0F/RT)$. However, because the Nernst equation is nearly valid on iron oxide surfaces in the triple-layer model, the decrease in the exponent for H^+ is essentially offset by the difference in the $\exp(-z\Psi_0F/RT)$ terms between reactions 2 and 13. Thus, the surface species identified by reaction 13 results in a mass law that is very similar to reaction 2. However, reactions 2 and 7 must be considered to be the best model because these surface species are consistent with the spectroscopic data. The experimental data (Ar system) and the model simulation with reaction 7 ($\log K = 26.548$) under argon are shown in Figure 3 (solid curve).

The spectroscopic data suggested that both bidentate binuclear and bidentate mononuclear surface species were formed. The best fits with these types of species individually were with reactions 2 and 7. There are insufficient experimental data to attempt a fit of the data with a combination of these species (data as a function of total arsenate concentration or total site density would be required). However, to see if it would improve the fit to the data, a combination of the bidentate binuclear reactions 7 and 10 were considered, but the combination yielded only a very small improvement in the fit (22.4) compared to reaction 7 alone (fit = 23.9). In these simulations, the protonated As(V) surface species (reaction 10) represented only a very small fraction of the adsorbed As(V), for example, $\sim 3.2\%$ at pH 4. Thus, the surface complexation modeling results suggest that adsorbed As(V) does not form a significant amount of protonated species at the hematite surface. The formation of nonprotonated As(V) surface species is supported by previous electrophoretic mobility studies that show that As(V) sorption decreases the zeta potential of iron oxide particles (10, 45). Moreover, ATR-FTIR investigations of phosphate adsorption complexes on amorphous iron oxides have demonstrated the formation of nonprotonated bidentate binuclear surface species at pH 7.5 (13), suggesting that arsenate can be expected to form similar bonds because of its similar chemistry.

On the basis of the good fit to the As(V) adsorption in the CO_2 -free Ar system with reaction 7 (Table 4), the model was then used to predict the effect of adsorbed carbonate on As(V) adsorption. The model predictions are shown as the dashed lines in Figure 3. The model predicts that the effects of carbonate are minimal in systems equilibrated with $P_{CO_2} = 10^{-3.5}$, with only a slight decrease in As(V) adsorption predicted at pH 7.75. The magnitude of the predicted decrease in As(V) adsorption (compared to the argon simulation) is similar to the actual decrease in As(V) adsorption measured experimentally at this pH. A greater decrease in As(V) adsorption is predicted for systems equilibrated with 1% P_{CO_2} . Although no experimental data were collected under these conditions, the prediction suggests that carbonate may increase the mobility of As(V) in groundwater systems,

TABLE 4. Fit of Various Arsenate Surface Reactions to Experimental Adsorption Data

species type	surface species	reaction	exponents in mass law defining surface species ^a					fit
			a	b	c	d	e	
bidentate mononuclear complexes	$\equiv\text{FeO}_2\text{AsO}_2^-$	1	1	2	1	-1	0	2820
	$\equiv\text{FeO}_2\text{AsO}_2^-$	2	1	2	1	0	-1	29.5
	$\equiv\text{FeO}_2\text{AsO}_2^-$	3	1	2	1	-0.1	-0.9	76.6
	$\equiv\text{FeO}_2\text{AsO}_2^-$	4	1	2	1	-0.2	-0.8	180
	$\equiv\text{FeO}_2\text{AsO}_2\text{H}$	5	1	3	1	0	0	4980
bidentate binuclear complexes	$(\equiv\text{FeO})_2\text{AsO}_2^-$	6	2	2	1	-1	0	2330
	$(\equiv\text{FeO})_2\text{AsO}_2^-$	7	2	2	1	0	-1	23.9
	$(\equiv\text{FeO})_2\text{AsO}_2^-$	8	2	2	1	-0.1	-0.9	57.1
	$(\equiv\text{FeO})_2\text{AsO}_2^-$	9	2	2	1	-0.2	-0.8	139
	$(\equiv\text{FeO})_2\text{AsO}_2\text{H}$	10	2	3	1	0	0	4810
monodentate complexes	$\equiv\text{FeOAsO}_3^{2-}$	11	1	1	1	-2	0	NC ^b
	$\equiv\text{FeOAsO}_3^{2-}$	12	1	1	1	0	-2	NC
	$\equiv\text{FeOAsO}_3^{2-}$	13	1	1	1	-1	-1	20.3
	$\equiv\text{FeOAsO}_3^{2-}$	14	1	1	1	-1.1	-0.9	26.8
	$\equiv\text{FeOAsO}_3^{2-}$	15	1	1	1	-0.9	-1.1	49.7
	$\equiv\text{FeOAsO}_3\text{H}^-$	16	1	2	1	0	-1	29.5
	$\equiv\text{FeOAsO}_3\text{H}_2$	17	1	3	1	0	0	4980

^a Mass law for formation of the surface species is $[\text{surface species}] = K_f[\equiv\text{FeOH}]^a(\text{H}^+)^b(\text{AsO}_4^{3-})^c \exp\{-F/RT(d\Psi_0 + e\Psi_\beta)\}$. ^b NC = no convergence.

because 1% P_{CO_2} (or greater) is typical of many aquifers (46). In the simulations for the systems under air or 1% P_{CO_2} , the predicted As(V) adsorption decreases primarily because the electrostatic potential of the β plane becomes increasingly negative as more carbonate is adsorbed. Free surface site concentrations remain relatively constant, and thus, the effect of competitive adsorption of carbonate on As(V) adsorption is negligible.

The simulated and experimental results can also be compared in terms of the amount of acid required to hold the pH constant as As(V) is adsorbed. For both the Ar and air-equilibrated systems, the simulations predict that more acid is needed to hold the pH constant at each pH value than was observed experimentally (Table 2). The results are consistent with the conclusion that the adsorbed As(V) forms a nonprotonated bidentate species, because either a monodentate species or a protonated bidentate species would increase the simulated acid consumption by more than an order of magnitude considering that the amount of arsenate adsorbed was generally $>10^{-4}$ mol/L for each experimental point. The simulated acid consumption was somewhat overestimated in comparison to the experimental values, and this may be due to the fact that the electrical double-layer properties of the hematite precipitate are somewhat different from those determined by Sahai and Sverjensky (44) (Table 3).

In this study, we combined adsorption kinetics, pseudo-equilibrium adsorption/titration experiments, EXAFS measurements, and surface complexation modeling to understand As(V) surface speciation and reactivity on hematite surfaces. The EXAFS analyses indicated that bidentate binuclear and bidentate mononuclear bonding mechanisms are preferred for As(V) adsorbed on hematite surfaces. At the chemical conditions in the kinetics experiments (4 g L^{-1} and $[\text{As}] = 1.5 \text{ mM}$), As(V) uptake was enhanced after 24 h at pH 4, 6, and 8. The enhancement of As(V) uptake was indirectly explained by differences in the ionic bond strength between the metal-carbonate and metal-hydroxyl bonds. A slight decrease in the As(V) adsorption rate observed at pH 7.75–8 at the early reaction time might be attributed to the greater negative charge at the surface caused by adsorbed carbonate. The pseudo-equilibrium adsorption data (1 g L^{-1} and $[\text{As}] = 0.5 \text{ mM}$) were modeled using SCM, and the results are consistent with the formation of nonprotonated bidentate arsenate surface species in both the ambient air and CO_2 -free Ar systems at pH 4–7.75. Overall, the macroscopic results

imply that the reaction conditions (e.g., total surface area in the system, pH, and P_{CO_2}) influence the dissolved and adsorbed carbonate concentrations, which in turn can alter the extent of As(V) uptake on hematite surfaces. Because the dissolved carbonate concentrations in groundwater are typically much higher than expected from equilibration with atmospheric P_{CO_2} , the sorption of carbonate ions may have a significant role in influencing As(V) transport processes at As-contaminated sites.

Literature Cited

- (1) Gao, S.; Tanji, K. K.; Goldberg, S. In *Symposium on Sources, Control, and Remediation of Oxyanions in Agroecosystems*; Dudley, L. M., Guitjens, J., Eds.; Proceedings, Symposium, Pacific Division; American Association for the Advancement of Science: San Francisco, CA, 1997.
- (2) Anderson, M. A.; Ferguson, J. F.; Gavis, J. J. *Colloid Interface Sci.* **1976**, *54*, 391.
- (3) Arai, Y.; Elzinga, E. J.; Sparks, D. L. *J. Colloid Interface Sci.* **2001**, *235*, 80.
- (4) Raven, K. P.; Jain, A.; Loeppert, R. H. *Environ. Sci. Technol.* **1998**, *32*, 344.
- (5) Xu, H.; Allard, B.; Grimvall, A. *Water, Air Soil Pollut.* **1988**, *40*, 293.
- (6) Fendorf, S. E.; Eick, M. J.; Grossl, P.; Sparks, D. L. *Environ. Sci. Technol.* **1997**, *31*, 315.
- (7) Manceau, A. *Geochim. Cosmochim. Acta* **1995**, *59*, 3647.
- (8) Waychunas, G. A.; Rea, B. A.; Fuller, C. C.; Davis, J. A. *Geochim. Cosmochim. Acta* **1993**, *57*, 2251.
- (9) Sun, X.; Doner, H. E. *Soil Sci.* **1998**, *163*, 278.
- (10) Suarez, D. L.; Goldberg, S.; Su, C. In *Mineral-Water Interfacial Reaction Kinetics and Mechanisms*; Sparks, D. L., Grundl, T. J., Eds.; ACS Symposium Series 715; American Chemical Society: Washington, DC, 1998; p 136.
- (11) Goldberg, S.; Johnston, C. T. *J. Colloid Interface Sci.* **2001**, *234*, 204.
- (12) Stumm, W. *Chemistry of the Solid-Water Interface: Processes at the Mineral-Water and Particle-Water Interface in Natural Systems*; Wiley: New York, 1993.
- (13) Arai, Y.; Sparks, D. L. *J. Colloid Interface Sci.* **2001**, *241*, 317.
- (14) Persson, P.; Nielsson, N.; Sjöberg, S. *J. Colloid Interface Sci.* **1996**, *177*, 263.
- (15) Tejedor-Tejedor, M. I.; Anderson, M. A. *Langmuir* **1990**, *6*, 602.
- (16) Stumm, W.; Morgan, J. J. *Aquatic Chemistry, Chemical Equilibria and Rates in Natural Waters*; Wiley: New York, 1995.
- (17) Feldkamp, J. R.; Shah, D. N.; Meyer, S. L.; White, J. L.; Hem, S. L. *J. Pharm. Sci.* **1981**, *70*, 638.

- (18) Zeltner, W. A.; Anderson, M. A. *Langmuir* **1988**, *4*, 469.
- (19) Su, C.; Suarez, D. L. *Clays Clay Miner.* **1997**, *45*, 814.
- (20) Wijnja, H.; Schulthess, C. P. *Soil Sci. Soc. Am.* **2002**, *66*, 1190.
- (21) Zachara, J. M.; Girvin, D. C.; Schmidt, R. L.; Resch, C. T. *Environ. Sci. Technol.* **1987**, *21*, 1.
- (22) Carrillo, A.; Drever, J. I. *Environ. Geol.* **1998**, *35*, 251.
- (23) Foster, A. L.; Brown, G. E., Jr.; Tingle, T. N.; Parks, G. A. *Am. Mineral.* **1998**, *83*, 553.
- (24) Jacobs, L. W.; Syers, J. K.; Keeney, D. R. *Soil Sci. Soc. Am. Proc.* **1970**, *34*, 750.
- (25) Livesey, N. T.; Huang, P. M. *Soil Sci.* **1981**, *131*, 88.
- (26) Sakata, M. *Environ. Sci. Technol.* **1987**, *21*, 1126.
- (27) Schwertmann, U.; Cornell, R. M. *Iron Oxides in the Laboratory: Preparation and Characterization*; VCH Publishers: Weinheim, Germany, 1991.
- (28) Ressler, T. J. *Synchrotron Radiat.* **1997**, *5*, 118.
- (29) Zabinsky, S. I.; Rehr, J. J.; Ankudinov, A.; Albers, R. C.; Eller, M. J. *Phys. Rev. B* **1995**, *52*, 2995.
- (30) Kitahama, K.; Kiriya, R.; Baba, Y. *Acta Crystallogr.* **1975**, *B31*, 322.
- (31) Herbelin, A. L.; Westall, J. C. A computer program for the determination of chemical equilibrium constants from experimental data, version 4.0, Oregon State University, 1999.
- (32) Nordstrom, D. K.; Archer, D. G. In *Arsenic in Ground Water: Geochemistry and Occurrence*; Welch, A. H., Stollenwerk, K. G., Eds.; Kluwer Academic Publishers: Boston, MA, 2003; p 1.
- (33) Bleam, W. F.; Pfeffer, P. E.; Goldberg, S.; Taylor, R. W.; Dudley, R. *Langmuir* **1991**, *7*, 1702.
- (34) Pierce, M. L.; Moore, C. B. *Water Res.* **1982**, *16*, 1247.
- (35) Fuller, C. C.; Davis, J. A.; Waychunas, G. A. *Geochim. Cosmochim. Acta* **1993**, *57*, 2271.
- (36) Bruno, J.; Stumm, W.; Wersin, P.; Brandberg, F. *Geochim. Cosmochim. Acta* **1992**, *56*, 1139.
- (37) Kohler, M.; Honeyman, B. D.; Leckie, J. O. *Radiochim. Acta* **1999**, *85*.
- (38) van Geen, A.; Robertson, A. P.; Leckie, J. O. *Geochim. Cosmochim. Acta* **1994**, *58*, 2073.
- (39) Villalobos, M.; Leckie, J. O. *J. Colloid Interface Sci.* **2001**, *235*, 15.
- (40) Wijnja, H.; Schulthess, C. P. *Soil Sci. Soc. Am. J.* **2001**, *65*, 324.
- (41) McBride, M. B. In *Environmental Chemistry of Soils*; Oxford University Press: New York, 1994; p 121.
- (42) Appelo, C. A. J.; Van der Weiden, M. J. J.; Tournassat, C.; Charlet, L. *Environ. Sci. Technol.* **2002**, *36*, 3096.
- (43) Wilkie, J. A.; Hering, J. G. *Environ. Sci. Technol.* **1971**, *5*, 657.
- (44) Sahai, N.; Sverjensky, D. A. *Geochim. Cosmochim. Acta* **1997**, *61*, 2801.
- (45) Matis, K. A.; Zouboulis, A. I.; Zamboulis, D.; Valtadorou, A. V. *Water, Air Soil Pollut.* **1999**, *111*, 297.
- (46) Hem, J. D. Water-supply paper; U.S. Geological Survey: Reston, VA, 1985; p 2254.

Received for review July 21, 2003. Revised manuscript received November 4, 2003. Accepted November 17, 2003.

ES034800W